JACS
JOURNAL OF THE AMERICAN CHEMICAL SOCIETY
Article
pubs.acs.org/JACS

Ligand-Assisted Enhancement of CO_2 Capture in Metal–Organic Frameworks

Roberta Poloni,[†,‡] Berend Smit,[†] and Jeffrey B. Neaton*[,‡]

[†]Department of Chemistry and Chemical and Biomolecular Engineering, University of California—Berkeley, Berkeley, California and [‡]Molecular Foundry, Lawrence Berkeley National Laboratory, Berkeley, California

Supporting Information

ABSTRACT: Using density functional theory with a van der Waals-corrected functional, we elucidate how CO_2 binds to a novel "BTT-type" metal–organic framework (MOF) featuring open metal centers. We show that CO_2 binds most favorably to open metal cation sites, but with an adsorption energy that can be three times more sensitive to the choice of the bridging ligand than to metal cation choice. A strong, three-site interaction between CO_2 and the open-metal site is predicted, with the binding energy enhanced by up to a factor of 2, depending on the ligand. The CO_2-MOF binding can be attributed to a combination of electrostatics and vdW dispersive interactions, both of which are critically sensitive to the local environment, and both of which contribute nearly equally to the overall binding strength. We show that a judicious choice of the organic linker and the metal center allows the binding energy to be tuned from 34.8 kJ/mol (for CaBTTri) to a maximum of 64.5 kJ/mol (MgBTT).

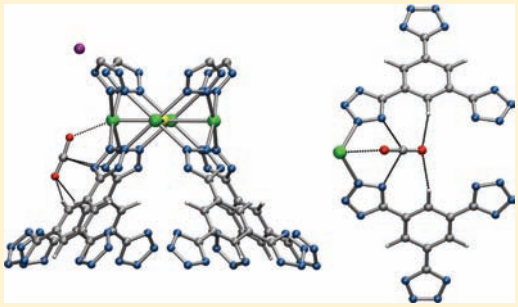

INTRODUCTION

Capturing and sequestering CO_2 is a route to partial mitigation of climate change associated with anthropogenic carbon dioxide emissions. Conventional CO_2 capture processes involve amine scrubbers that require a large heat of regeneration, resulting in losses of 25–40%.[1,2] New means of CO_2 separation from flue gas are clearly needed. Among candidate alternative methods for CO_2 separation, physisorption via metal–organic frameworks (MOFs) is one of the most promising,[3−6] although the issue of stability of these materials toward water vapor represents a significant limiting factor and it is a very active field of research in the MOF community.[7−10] MOFs are three-dimensional nanoporous extended solids composed of metal centers connected by organic molecules (called bridging ligands or linkers). A broad range of ligand–metal center combinations are synthetically accessible,[6,11] and thus MOFs can comprise an ideal palette for materials design and optimization, provided sufficient understanding of CO_2 uptake mechanism is available. MOFs exhibiting coordinatively unsaturated metal centers have been observed to provide an exceptional selectivity of CO_2 over N_2,[12] which is determinant for an efficient gas separation from a postcombustion process. Several studies have quantified how the CO_2 heat of adsorption changes when replacing the metal atom for a given MOF topology.[12−16] However, the manner in which metal center-CO_2 binding may be affected by bridging ligands remains an underexplored and open question. Given the wide variety of ligands available through conventional synthesis, there is significant opportunity to tune CO_2-MOF interactions using different ligands.

In this work, we use density functional theory-based calculations to study a class of recently synthesized sodalite-type frameworks (BTT-type frameworks)[17−20] with coordinatively unsaturated metal centers which, for certain metal centers, have shown promising selectivity of CO_2 over N_2. Compared to other MOFs with open metal sites, BTT-type framworks have more flexibility as they also feature extraframework cations. In order to quantitatively describe the CO_2-MOF binding, we adopt recently developed methods to account for van der Waals (vdW) interactions[21−23] within DFT. While most prior computational studies have focused on metal center–CO_2 interactions,[13,15,16,24] here we focus on CO_2 binding as a function of both bridging ligand and metal center, quantifying the contribution of the linker to the CO_2 affinity for the open metal site. Remarkably, we find that in open metal BTT-type frameworks, the CO_2 binding can be significantly more sensitive to the organic linker choice than the metal center, depending on the metal site cation. We further predict how recently measured heats of adsorption of 21 kJ/mol for Cu sites in BTTri-MOFs[19] might be significantly tuned upon cation and organic linker substitution leading to binding energies of of up to 64.5 kJ/mol in MgBTT, highly promising for an efficient adsorption/desorption process.[25] The understanding developed here can lead to new routes to higher adsorbate binding energies in MOFs through coordinated computational design of both optimal metal centers *and* bridging ligands.

Received: December 21, 2011
Published: March 30, 2012

   dx.doi.org/10.1021/ja2118943 | *J. Am. Chem. Soc.* 2012, 134, 6714–6719

COMPUTATIONAL DETAILS

Our DFT calculations are performed within the generalized gradient approximation (GGA) of Perdew, Burke, and Ernzerhof (PBE). For Mg, Ca, and Sr frameworks, we use a recent nonlocal functional (vdW-DF)[22] which captures long-range dispersion forces; for CuBTT, which is antiferromagnetic, long-range dispersion forces are described with a semiempirical approach proposed by Grimme[23] (PBE+D), which is considered to be equally accurate for CO_2-MOF binding.[26] All calculations are performed with the SIESTA package[27] and those using vdW-DF rely on the implementation of Román-Pérez and Soler.[28] We use variationally optimized[29,30] double-ζ polarized basis sets (implying the presence of d-orbitals) for C, N, and O atoms. Basis sets optimized with vdW-DF are employed for both PBE and vdW-DF calculations. Trouiller-Martins pseudopotentials are used, with 2s and 2p electrons of C, N, and O atoms explicitly included in the valence. For all metal atoms studied, semicore electrons are also included (e.g., 2s, 2p, and 3s for Mg; 3s, 3p, and 4s for Ca). Real space integrals are performed on a mesh with a 300 Ry cutoff. Geometries are optimized until Hellmann–Feynman forces are smaller than 20 meV/Å. For all reported adsorption energies, a counterpoise correction is applied to correct for basis set superposition error (BSSE). The accuracy of our local basis is checked by comparing BSSE-corrected binding energies with those obtained using plane waves with the VASP package.[31] VASP-PBE calculations are peformed using PAW pseudopotentials, with a plane-wave energy cutoff of 500 eV. For a given configuration, values of 38.6 and 38.0 kJ/mol are obtained, with SIESTA and VASP, respectively, and corresponding O–C–O bond angles are 173.9° and 174.6°, respectively. Adsorption energies are computed at zero temperature and neglect zero-point energy contributions. We have recently shown[26] that calculated thermal contributions at room temperature, together with zero-point energies, lower the CO_2 adsorption energy in CaBTT by about 5 kJ/mol.

STRUCTURE

Our study focuses on sodalite-based MOFs of the form $M'_3[(M_4Cl)_3(BTT)_8]_2$, recently synthesized frameworks with M = Mn, Fe, and Cu.[17,18,20] In Figure 1, we present the structure of this MOF, where the fundamental building block of this structure is a truncated octahedron consisting of six $[M_4Cl]^{7+}$ squares connected by eight BTT^{3-} ligands. The truncated octahedra share square faces, generating a cubic framework structure with space group $Pm\bar{3}m$. The metal centers (M in the formula) are initially octahedrally coordinated by a dimethylformamide solvent molecule that is later removed, leading to coordinatively unsaturated metal centers and a total of 207 atoms per primitive cell. The overall anionic charge of the framework is balanced by additional extraframework metal atoms (M′ in the formula). In general, they are the same type of atom as the metal center with a stoichiometry of 3 M′ atoms per 2 primitive cells, as shown by the above formula. Two sites for the M′ atoms have been observed: one positioned inside the sodalite cage-like units (within the truncated octahedra) having 4-fold symmetry (6*e* Wyckoff position),[20] and the other coodinated to two N atoms of two tetrazolate rings in a chelated coordination geometry (24*k* Wyckoff position),[17,18] as shown in Figure 1. There are two inequivalent N atoms at the 48*n* Wyckoff position: those closer to the cations (which we call N1, see Figure 1) and those coordinated to the C atom (N2). In what follows, we consider M = Mg, Cu, Ca, and Sr and M′ = Li, Na, and K. We use monovalent M′ cations to reduce computational cost and simultaneously enforce charge neutrality.

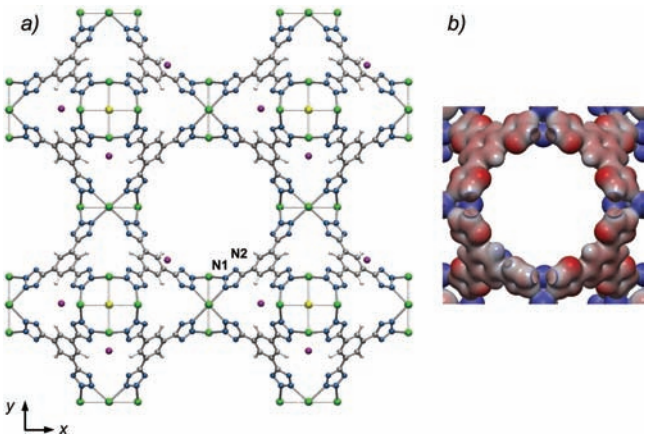

Figure 1. Left panel: Crystal structure of CaBTT. A 2 × 2 × 2 supercell is shown, including a cube of eight solidate-like truncated octahedral cages sharing square faces. Ca, Na, Cl, C, and N, atoms are shown in green, purple, yellow, silver, and blue, respectively. The right panel shows the electrostatic potential surface on a single unit cell plotted on the isovalue of the charge density of 0.03 electrons/au^3. Red and purple regions correspond to negative and positive electrostatic potential, respectively.

CaBTT MOF. We first compute relative energies of CaBTT MOFs with M′ atoms in different arrangements, in order to establish their location, starting from experimental atomic coordinates[32] at both Wyckoff positions. For M′ = Li, Na, and K, we optimize the structure in each case. After optimization, the crystal symmetry is lowered to monoclinic, with angles deviating from 90° by up to 0.3%, depending on M′. We find that having the M′ atoms at the 24*k* Wyckoff position results in a larger cohesive energy (by about 50 kJ/mol) compared to the M′ atoms at the 6*e* position. Thus, in the following, all calculations are performed with M′ atoms at the 24*k* position and M′ = Na (unless specified otherwise).

Averaging over four different M′ atoms orderings to account for the statistical distribution of the 3 M′ atoms over the 24 sites, the computed average lattice parameters of $Na_3[(Ca_4Cl)_3(BTT)_8]$ are 19.76 Å (PBE) and 19.93 Å (vdW-DF). To compare with experiment, we scale the reported lattice parameter of 19.81 Å for unsolvated CaBTT,[32] with Ca atoms as extraframework cations, to account for our different extraframework cation choice. We first compute the lattice constant of CaBTT as a function of the ionic size of different M′ atoms (Li, Na, K). Then, with the obtained linear function which reproduces the lattice parameter as a function of Shannon ionic radii, we rescale the experimental value (M′ = Ca in the experiment). In addition, a 0.56% lattice parameter expansion[18] due to the presence of solvent is considered. The rescaled value is 19.69 Å, which compares well with our calculations.

The presence of M′ atoms modifies the local potential in their vicinity. When M′ atoms are coordinated by two N2 atoms, both N1 and N2 atoms have approximatively the same Mulliken charge (see Figure S1 in Supporting Information). In absence of M′ atoms in our calculation, the charge is balanced by additional electrons, and a factor of 2 difference is found between the partial charge of N1 compared to N2, with N1 being more negatively charged. Additionally, the presence of M′ atoms removes degeneracies within the electronic structure, resulting in wave functions no longer delocalized over the unit cell and instead exhibiting a localized defect-like character (see Figure S2 in Supporting Information).

dx.doi.org/10.1021/ja2118943 | J. Am. Chem. Soc. 2012, 134, 6714–6719

RESULTS AND DISCUSSION

CaBTT–CO_2 Interactions. In Figure 1b, we show a representative electrostatic potential isosurface of the CaBTT MOF with M′ = Na. The isosurface shows regions of positive and negative potential and rather clearly suggests two candidate sites where CO_2 is likely to bind: (i) regions of positive potential near the open metal sites (site A), which may attract a CO_2 molecules's oxygen atoms; and (ii) the negatively charged N2 atoms of the tetrazole molecule, where CO_2 may bind via the carbon atom (site B). In what follows, we introduce a single CO_2 molecule near these two sites, relax the structure, and explore binding energetics.

Relaxed DFT-PBE CO_2 binding geometries are reported in Figure 2. (Optimized atomic coordinates are reported in the Supporting Information.) After relaxation, the two initial binding geometries dicussed above differ only by a 60° rotation around the *y*-axis (see Figure 2), and the vdW-DF (PBE) Ca–O–C angle changes from 156.2° (152.9°) to 129.1° (132.4°) after binding with the ligand. The A site configuration corresponds to CO_2 binding in an end-on mechanism, with one neighboring M′ atom located at the A1 site (see Figure 2b); the simultaneous electrostatic attraction of the CO_2 oxygen with the Ca open metal site and a nearby M′ atom enhances the binding (see Figure 2a). In absence of a neighboring M′ atom, the binding energy is 23.3 kJ/mol (PBE). Interestingly, we observe a significantly stronger CO_2 binding at the B site of 62.0 kJ/mol (43.1 kJ/mol) with vdW-DF (PBE). The enhanced adsorption at the B sites results from a novel 3-fold binding configuration: the CO_2 O atoms interact with both the H and Ca atoms of the framework, respectively, while the CO_2 C atom is concomitantly attracted to the negatively charged N of the tetrazole ligand. This is qualitatively different from the commonly considered open metal site mechanism, where only the Ca–O interaction is thought to contribute to the binding. In this case, the proximity of the tetrazole ligand enhances the CO_2–MOF interaction by up to 50%. Nudged elastic band calculations showed the absence of an energy barrier between the two configurations (see Figure S3 of the Supporting Information). Hence, in what follows, we report binding energies at the B site only.

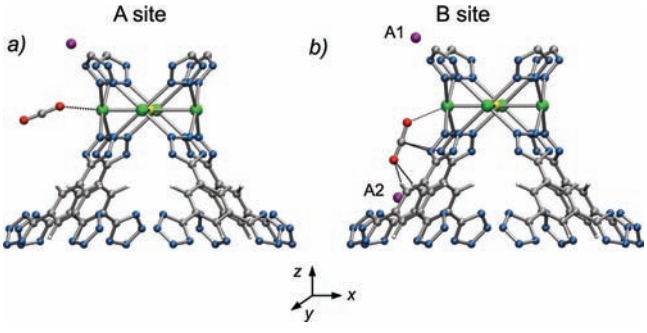

Figure 2. CO_2–CaBTT binding configurations at the (a) A and (b) B sites. C–N, O–Ca, and O–H bond distances computed with PBE are 2.789, 2.476, and 2.656 Å at the B site, while the O–Ca bond distance at the A site is 2.554 Å. These values correspond to a binding geometry with one M′ atom at the A1 site, and other two M′ atoms not shown here. The M′ atom at the A2 site is also shown.

The relatively large CO_2 binding energy predicted here is accompanied by a significant induced dipole moment, reflected in a deviation of the O–C–O bond angle from 180°. We compute the CO_2 induced dipole moment by integrating the first moment of the difference in charge density between the MOF + CO_2 system and the isolated MOF and CO_2 constituents, for fixed geometry. The bending angle and induced dipole (for the B site with M′ at A1) are 174.0° (173.8°) and 0.567 D (0.622 D) with vdW-DF (PBE). Accordingly, the C–O bond length involving the O closer to Ca is found to be larger, 1.201 Å (1.194 Å), compared to the other C–O bond distance, 1.173 Å (1.169 Å), with vdW-DF (PBE). The amount of charge transfer is also estimated by integrating the charge density difference; negliglible values are obtained with both functionals. The MOF evidently polarizes CO_2, inducing a dipole with negligible charge transfer. van der Waals dispersion corrections are significant but do not affect the magnitude of the induced dipole or O–C–O bond angle.

In addition to the ligands, the M′ atoms can also significantly affect CO_2-MOF binding due to local modifications of the electrostatic potential, as discussed above. Different M′ arrangements for a given CO_2 binding site lead to differences in adsorption of up to 30 kJ/mol (PBE). After exploring four orderings of M′ = Na (see Supporting Information), we observe that the sites with the largest binding energies are those reported in Figure 2 with one M′ atom at A2 site. Here, as in the A site case for M′ at A1, the simultanous electrostatic attraction of the CO_2 oxygen with the Ca open metal site and M′ enhances the binding, resulting in E_{ads} = 48.5 kJ/mol (PBE). Similar results have been found experimentally in H_2 adsorption measurements of a related MOF, MnBTT, where the H_2 binding site exhibiting stronger electrostatic interaction has a close M′ = Mn.[33] When both Ca-neighboring linkers have an M′ cation at the A1 site, the CO_2–MOF interaction has no contribution from the ligand and E_{ads} = 20.3 kJ/mol (PBE). In this case, the CO_2 molecule interacts in a end-on mechanism with the Ca–O–C angle being approximately 180°. When the M′ atoms are not in the A1 nor in the A2 site, a binding energy of 35.6 kJ/mol (PBE) is found. In what follows, the CO_2 binding geometry with M′ at the A1 site will be considered unless specified.

Role of the Linker and the Metal Centers on the CO_2 Adsorption Energy. As discussed above, we find that the BTT ligands can strongly enhance the CO_2 interaction with open metal sites. To further explore the role of ligands on CO_2 adsorption, we compute binding geometries and energetics after substituting N with O (oxazole) and CH (triazole), as shown in Figure 3. Calculated binding energies, bond lengths, and bond angles are reported in Table 1. We observe that, in both cases, the interaction energy is reduced compared to the BTT ligand (tetrazole). For triazole, the adsorption energy is dramatically reduced compared to the tetrazole case, E_{ads} = 34.8 kJ/mol (23.4 kJ/mol) with vdW-DF (PBE), with the CO_2 molecule pointing toward the center of the pore in a geometry reminiscent of the A site binding geometry. This is reflected by the bond distances reported in Figure 3, and indicates a reduced interaction with the linker. Empirically, the triazolate rings are known to be arranged randomly throughout the structure.[19] Accordingly, we also compute the CO_2 binding energy in a geometry where the CH of the triazole faces an N of tetrazole (Figure 3). We find that the CO_2 molecule approaches the tetrazole N2 atom, resulting in a binding energy of 50.3 kJ/mol (31.3 kJ/mol) with vdW-DF (PBE).

A different scenario is observed for the oxazole linker. Due to the presence of an additional valence electron (compared to BTT) and lack of experimental structural data for this crystal,

dx.doi.org/10.1021/ja2118943 | J. Am. Chem. Soc. 2012, 134, 6714–6719

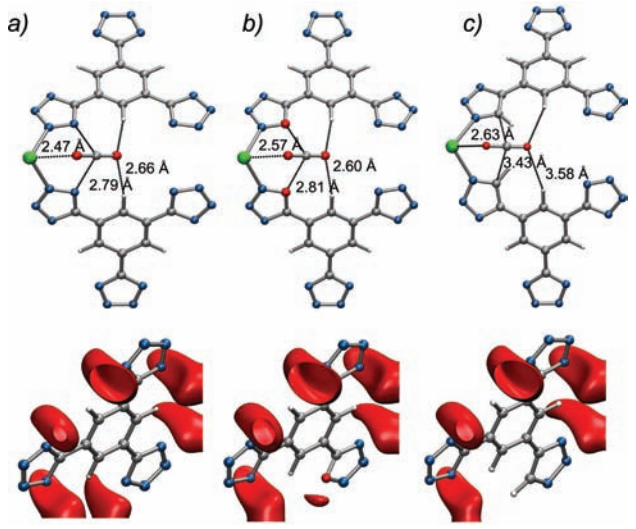

Figure 3. Binding geometry for the (a) tetrazole, (b) oxazole, and (c) triazole linkers. The bond lengths correspond to PBE results. The lower panels show the electrostatic potential isosurface plotted at 0.065 Ry. Larger partial negative charges are found for N compared to O.

Table 1. CO_2 Adsorption Energies Obtained with vdW Dispersion Corrections (vdW-DF) for the Different Bridging Ligands[a]

ligand	E_{ads}(kJ/mol)	O−C−O (deg)	O−M (Å)	O−C/N/O (Ang)	ΔE (%)
tetrazole	62.0 (43.1)	173.8	2.476	2.789	36
triazole	34.8 (23.4)	179.5	2.627	3.403	40
triazole[b]	50.3 (31.3)	173.6	2.545	3.124	48
oxazole	54.9 (31.0)	177.6	2.516	2.816	56

[a]PBE binding energy is shown in brackets; PBE bond distances and O−C−O bond angles are also reported. ΔE is the relative energy difference between vdW-DF and PBE. [b] Geometry of the triazole facing a tetrazole.

two different set of calculations are performed: (i) one with an additional electron (and accompanying uniform positive background) and (ii) another with an addition of an H atom at the benzene molecule. The resulting binding energies vary for the two calculations only 6%. The computed CO_2−MOF binding energy is 54.9 kJ/mol (31.0 kJ/mol), with vdW-DF (PBE). (These values are obtained with the additional H atom.) The presence of the oxygen lone pairs does not enhance the CO_2 interaction, as expected. The larger negative partial charge on the N compared to O is instead responsible for the stronger interaction with the linker, as reflected by the electrostatic potential surface (lower panels of Figure 3). The existence of regions with negative electrostatic potential is confirmed by the experimental observation of M′ atoms situated in these regions (24*k* position).[17] The ΔE between vdW-DF and PBE binding energies for the ligands explored here is reported in Table 1. The oxazole in found to exhibit the largest ΔE, consistent with the presence of highly polarizable lone pairs. The relatively small O−C−O angle found for the oxazole molecule reflects a smaller electrostatic interaction compared to tetrazole.

The extraframework M′ (Li, Na, K) and framework M (Mg, Cu, Ca, Sr) cations can also affect the CO_2 binding energy and thus the ability of the MOF to capture CO_2. In both cases, smaller cations increase the interaction energy with CO_2. Binding energies and geometries, as a function of M′ at the A1 and A2 sites, are reported in the Supporting Information. Our results are consistent with the increase in enthalpy of adsorption of H_2 measured for cations with smaller ionic radii in extraframework cation-exchanged variants of the MnBTT framework.[33] When changing the cation at the open metal site, the interaction energy increases by ∼10 kJ/mol with a reduction in size from Sr to Mg, excluding Cu, whose binding mechanism with CO_2 is somewhat different and described below. For Mg, Ca, and Sr, smaller ionic radii result in stronger electrostatic interactions with O, and the larger induced dipole in turn increases electrostatic interactions between CO_2 and the N2 atoms. Smaller O−H bond lengths are found for larger cations due to increased proximity to the open metal cation. In Table 2, we show MOF−CO_2 bond distances for all M-BTT systems studied, along with their corresponding bond angles and interaction energies. Larger bond angles are found for smaller cations, confirming the electrostatic nature of the interaction. However, although the Shannon radius of Cu is similar to that of Mg, the CO_2 binding energy is significantly less for CuBTT than MgBTT. This is due to the more covalent character of the metal−ligand bonding in CuBTT, as reflected by a shorter metal−ligand bond length (M−N is 2.038 Å for Cu and 2.140 Å for Mg) and smaller Mulliken charge (0.75 for Cu and 1.45 for Cu). Significant hybridization between Cu d orbitals and N p orbitals can explain the reduced Cu charge and therefore the reduced affinity of Cu for CO_2. Independent of framework cation, the vdW dispersion corrections increase binding energies by about 20 kJ/mol (or 40%) over PBE (see Table 2). For Mg, Ca, and Sr, binding energies are computed using vdW-DF, while PBE+D is employed for Cu.

Our calculated CO_2 binding energies for the Cu framework compare well with the available experimental isosteric heat of adsorption of CO_2 measured for CuBTTri.[19] Adsorption energies reported below are vdW dispersion corrected (PBE +D). For the bare Cu framework we find an antiferromagnetic ground state within the $[Cu_4Cl]^{7+}$ complexes, with a magnetic moment per copper of 0.54 μ_B, also in agreement with experimental observations.

At this point, it is important to mention that how the triazole molecules are oriented relative to each other has yet to be

Table 2. CO_2 Adsorption Energies Obtained with vdW Dispersion Corrections for Different Metal Ions[a]

M	E_{ads} (kJ/mol)	O−C−O (deg)	O−M (Å)	C−N (Å)	O−H (Å)	O−M′ (Å)	ΔE (%)
Mg	64.5 (44.4)	171.6	2.238	2.687	2.647	4.322	37
Cu	34.5 (15.7)	176.1	2.753	2.831	2.530	3.985	75
Ca	62.1 (43.1)	173.8	2.476	2.789	2.656	5.065	36
Sr	55.2 (36.0)	175.5	2.657	2.890	2.493	5.450	42

[a]vdW-DF is used for Mg, Ca, and Sr, while PBE+D is used for Cu, as explained in the text. PBE adsorption energies are in brackets. ΔE is the relative energy difference between vdW-DF and PBE. PBE bond distances and the O−C−O bond angle of CO_2 are reported for all cases.

dx.doi.org/10.1021/ja2118943 | J. Am. Chem. Soc. 2012, 134, 6714−6719

determined experimentally. Three different orientations are possible, CH−CH (a CH group of one molecule facing the CH group in the neighboring one, as shown in Figure 3), CH−N, and N−N. We compute the binding energy of CO_2 in each case and find significanly different values depending on the orientation of the molecules, consistent with results discussed above for CaBTT. For the Cu framework, our vdW-corrected CO_2 binding energies are 21.7 kJ/mol for ligands in a CH−CH orientation, and 34.5 and 9.7 kJ/mol for N−N and CH−CH arrangements, respectively. However, experimentally, the heat of adsorption as a function of loading is found to be constant (21 kJ/mol);[19] taken together with our calculations, this indicates that the CH−CH arrangement dominates the experimental structure, since if N−N and CH−CH arrangements were to coexist, a loading-dependent heat of adsorption would be observed. Further support for a CH−N experimental structure is that the calculated energy difference between forming a pair of ligands in CH−CH and N−N orientations, relative to two CH−N arrangements, is a factor of 2 larger (6.6 kJ/mol) than the temperature associated (100 °C) with the CuBTTri synthesis[19] (3.3 kJ/mol). Therefore, we may conclude that the CO_2 binding energy of 21.7 kJ/mol for a CH−N arrangement is in excellent agreement with the experimental value of 21 kJ/mol.[19] As a further validation of our study, we recently showed that the heat of adsorption of CO_2 in MOF-74, computed with the same methodologies employed in this work, is in very good agreement with experimentally reported values.[26]

CONCLUSIONS

In this work, we have used density functional theory-based calculations, including van der Waals dispersion corrections, to show that the choice of the ligand is crucial in determining CO_2 binding energetics in MOFs. For BTT-type MOFs, depending on the organic ligand, the occurrence of a strong three-site interaction between the CO_2 and the framework can significantly enhance (up to 50%) the strong affinity of the open metal site for CO_2. CO_2-MOF binding is dominated by electrostatics, the energy difference between PBE and vdW-DF (which is related to the vdW contribution) is 36−75%, depending on the local environment around CO_2. By exploring different choices for both the open metal sites (Mg, Cu, Ca, and Sr) and extraframework cation (Li, Na, K), we show and quantify that, in both cases, smaller cations increase the electrostatic interaction with CO_2. Interestingly, the Cu framework provides a significantly reduced affinity for CO_2 compared to the other metals, due to its reduced positive charge. Additionally, stronger electrostatic interactions with CO_2 are found for linkers with atoms having larger negative partial charges, i.e., for oxazole and tetrazole. In particular, the CO_2 adsorption energy can by enhanced by almost a factor of 2 by replacing triazole with tetrazole (35.8 kJ/mol versus 62.0 kJ/mol). Interestingly, the CO_2 binding is 3 times more sensitive to the organic linker ($\Delta E \approx 30$ kJ/mol) compared to the metal atom choice ($\Delta E \approx 10$ kJ/mol). By combining the metal center and the ligand providing the larger affinity for CO_2, a strong interaction of 64.5 kJ/mol obtained for MgBTT, placing this MOF among the most promising compounds to be used for carbon capture.

ASSOCIATED CONTENT

Supporting Information

Mulliken population analysis; Electronic band structure; Nudged elastic band result; Atomic coordinates of PBE relaxed structure of CaBTT + CO_2, MgBTT + CO_2, CuBTT + CO_2, SrBTT + CO_2, CaBTT(oxazole) + CO_2 and CaBTT(triazole) + CO_2. This material is available free of charge via the Internet at http://pubs.acs.org.

AUTHOR INFORMATION

Corresponding Author

jbneaton@lbl.gov

Notes

The authors declare no competing financial interest.

ACKNOWLEDGMENTS

We thank G. Galli for fruitful discussions and for carefully reading the manuscript. We also thank J. R. Long, E. Bloch, and K. Sumida for sharing data on BTT-type MOFs. R.P. thanks P. Doak and D. Prendergast for discussions. This work was supported by the Center for Gas Separations Relevant to Clean Energy Technologies, an Energy Frontier Research Center funded by the U.S. Department of Energy, Office of Science, Office of Basic Energy Sciences under Award No. DE-SC0001015. Work at the Molecular Foundry was supported by the Office of Science, Office of Basic Energy Sciences, of the U.S. Department of Energy under Contract No. DE-AC02-05CH11231. Computational resources were provided by DOE (NERSC, LBNL Lawrencium).

REFERENCES

(1) *IPCC, IPCC Special Report on Carbon Dioxide Capture and Storage*; Cambridge University Press: Cambridge, 2005.
(2) Haszeldine, R. S. *Science* **2009**, *325*, 1647.
(3) Millward, A. R.; Yaghi, O. M. *J. Am. Chem. Soc.* **2005**, *127*, 17998.
(4) Ferèy, G. *Chem. Soc. Rev.* **2008**, *37*, 191.
(5) Morris, R. E.; Wheatley, P. S. *Angew. Chem., Int. Ed.* **2008**, *47*, 4966.
(6) D'Alessandro, D. M.; Smit, B.; Long, J. R. *Angew. Chem., Int. Ed.* **2010**, *49*, 6058.
(7) Armstrong, G. *Nat. Chem.* **2009**, *1*, 682.
(8) Cychosz, K. A.; Matzger, A. J. *Langmuir* **2010**, *26*, 17198.
(9) Yang, J.; Grzech, A.; Mulder, F. M.; Dingemans, T. J. *Chem. Commun.* **2011**, *47*, 5244.
(10) Liu, J.; Thallapally, P. K.; McGrail, B. P.; Brown, D. R.; Liu, J. *Chem. Soc. Rev.* **2012**, *41*, 2308.
(11) James, S. L. *Chem. Soc. Rev.* **2003**, *32*, 276.
(12) Britt, D.; Furukawa, H.; Wang, B.; Glover, T. G.; Yaghi, O. M. *Proc. Natl. Acad. Sci. U.S.A.* **2009**, *106*, 20637.
(13) Caskey, S. R.; Wong-Foy, A. G.; Metzger, A. J. *J. Am. Chem. Soc.* **2008**, *130*, 10870.
(14) Dietzel, P. D. C.; Johnsen, R. E.; Fjellvåg, H.; Bordiga, S.; Groppo, E.; Chavan, S.; Blom, R. *Chem. Comm.* **2008**, 5125.
(15) Bloch, E. D.; Britt, D.; Lee, C.; Doonan, C. J.; Uribe-Romo, F. J.; Furukawa, H.; Long, J. R.; Yaghi, O. M. *J. Am. Chem. Soc.* **2010**, *132*, 14382.
(16) Valenzano, L.; Civellari, B.; Sillar, K.; Sauer, J. *J. Phy. Chem. C* **2011**, *115*, 21777.
(17) Dincă, M.; Dailly, A.; Liu, Y.; Brown, C. M.; Neumann, D. A.; Long, J. R. *J. Am. Chem. Soc.* **2006**, *128*, 16876.
(18) Dincă, M.; Han, W. S.; Liu, Y.; Dailly, A.; Brown, C. M.; Long, J. R. *Angew. Chem., Int. Ed.* **2007**, *46*, 1419.
(19) Demessence, A.; D'Alessandro, D.; Foo, M. L.; Long, J. R. *J. Am. Chem. Soc.* **2009**, *131*, 8784.

(20) Sumida, K.; Horike, S.; Kaye, S. S.; Herm, Z. R.; Queen, W. L.; Brown, C. M.; Grandjean, F.; Long, G. J.; Dailly, A.; Long, J. R. *Chem. Sci.* **2010**, *1*, 184.
(21) Dion, M.; Rydberg, H.; Schroder, E.; Langreth, D. C.; Lundqvist, B. I. *Phys. Rev. Lett.* **2004**, *92*, 246401.
(22) Lee, K.; Murray, E. D.; Kong, L.; Lundqvist, B. I.; Langreth, D. C. *Phys. Rev. B* **2010**, *82*, 081101(R).
(23) Grimme, S. *J. Comput. Chem.* **2006**, *27*, 1787.
(24) Wu, D.; Xu, Q.; Liu, D.; Zhing, C. *J. Phys. Chem. C* **2010**, *114*, 16611.
(25) Berger, A. H.; Bhown, A. S. *Energy Procedia* **2011**, *4*, 562.
(26) Poloni, R.; Smit, B.; Neaton, J. B. *J. Phys. Chem. C* 2012, submitted.
(27) Soler, J. M.; Artacho, E.; Gale, J. D.; García, A.; Junquera, J.; Ordejón, P.; Sanchez-Portal, D. S. *J. Phys: Condens. Matter* **2002**, *14*, 2745−2779.
(28) Roman-Perez, G.; Soler, J. M. *Phys. Rev. Lett.* **2009**, *103*, 096102.
(29) Junquera, J.; Paz, O.; Sánchez-Portal, D.; Artacho, E. *Phys. Rev. B* **2001**, *64*, 235111.
(30) Anglada, E.; Soler, J. M.; Junquera, J.; Artacho, E. *Phys. Rev. B* **2002**, *66*, 205101.
(31) Kresse, G.; Furthmüller, J. *Phys. Rev. B* **1996**, *54*, 11169.
(32) Sumida, K.; Long, E. B., *private communication*, 2010.
(33) Dincă, M.; Long, J. R. *J. Am. Chem. Soc.* **2007**, *129*, 11172.